ELECTROSTATICALLY SUSPENDED AND SENSED MICRO-MECHANICAL RATE GYROSCOPE

R. Torti, M. Gerver, V. Gondhalekar, S. Bart, B. Maxwell
SatCon Technology Corporation
12 Emily Street
Cambridge, MA 02139

SUMMARY

The goal of this work is development of fully electrostatically suspended and rebalancing angular rate sensing micro-gyroscope fabricated according to standard VLSI techniques. Fabrication of test structures is proceeding. Off chip electronics for the electrostatic sensing and driving circuits has been tested. The prototype device will be assembled in a hybrid construction including the FET input stages of the sensors.

INTRODUCTION

SatCon Technology is currently in the design and fabrication phase of a proof of principle, fully electrostatically suspended and rebalancing angular rate sensing micro-gyroscope. The structure will be fabricated according to current VLSI micromachining methods. Performance targets include angular rate sensitivity of 0.01°/s at 100 Hz for 8.3 kHz (revolutions/s) spin rate. The program is supported under contract by NASA-Langley Research Center (# NAS1-19590) as a Phase II SBIR.

To date, a set of test microstructures designed in-house has been fabricated by a VLSI supplier, prototype capacitive sensing electronics and rotor drive electronics have been tested, and the design and analysis of structures suitable for a prototype gyro is underway.

APPROACH

Micro-electronic fabrication technologies have recently been applied to produce novel micro-mechanical devices such as motors, pressure sensors, and linear actuators. Their small size, integration compatibility with electronic circuits, and potential low cost invite research. The micro-mechanical gyroscope, proposed for this research effort, is a device that would have application to aerospace, commercial, and military systems. The final instrument goal is shown in Figure 1 and would consist of entirely integrated electronics and RF signal transmitter and lithium battery for a long-life, wireless accelerometer and rate sensor.

The prototype goal for this work, however, is more modest. As shown in Figure 2, the

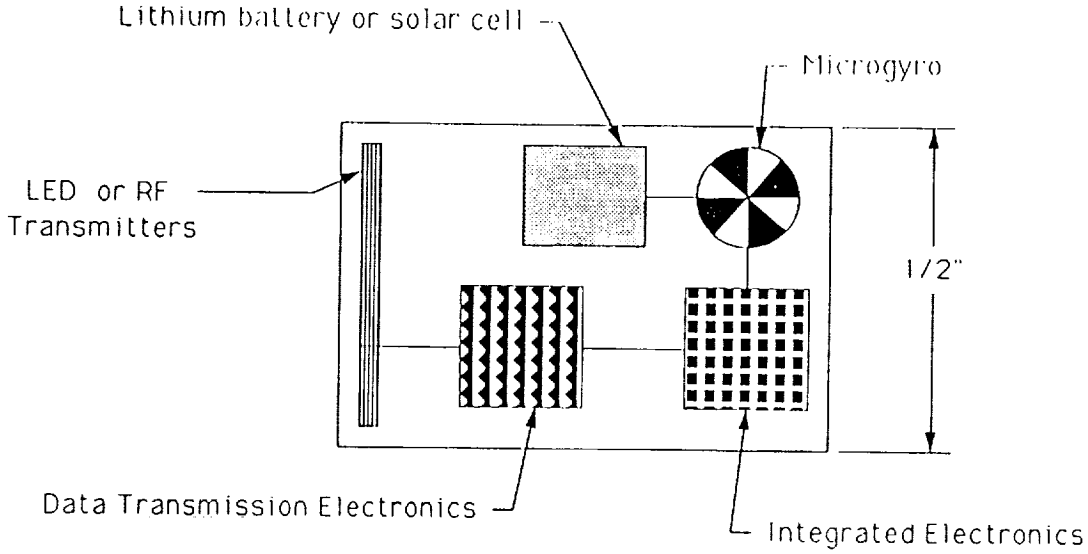

Figure 1. Integrated Microgyro Concept.

mechanical gyro structure would consist of a VLSI fabricated multi-layer polysilicon. The essential geometry is a circular disc rotating at 8 kHz and driven, suspended, rebalanced, and sensed completely electrostatically. This structure or set of structures will be at the center of and connected to a hybrid structure which includes the FET front ends of the capacitive sensor set. Drive electronics and the sensor filters and demodulators will be off chip.

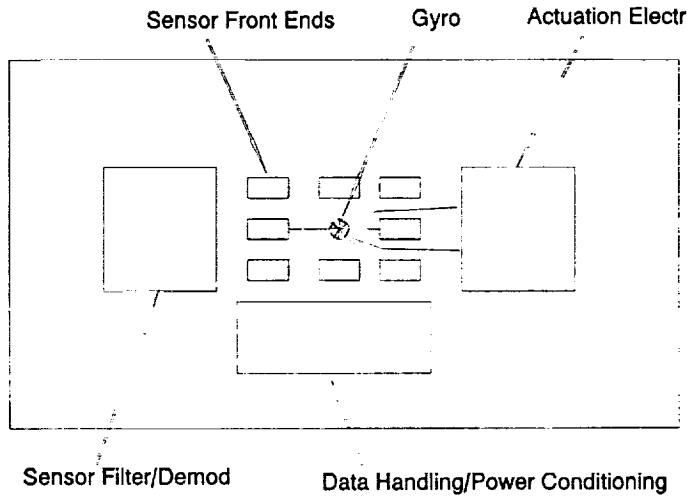

Figure 2. Configuration of Prototype Micro-Gyro.

A "rebalanced" gyroscope has a control system designed to hold the gyro in a constant position while it is subject to external forces. Since the controlled mass (the gyro rotor in this case) is held to a nearly constant position, the linearity of the sensors and actuators is improved, and the overall dynamics are simplified. A block diagram of the gyro system is shown in Figure 3.

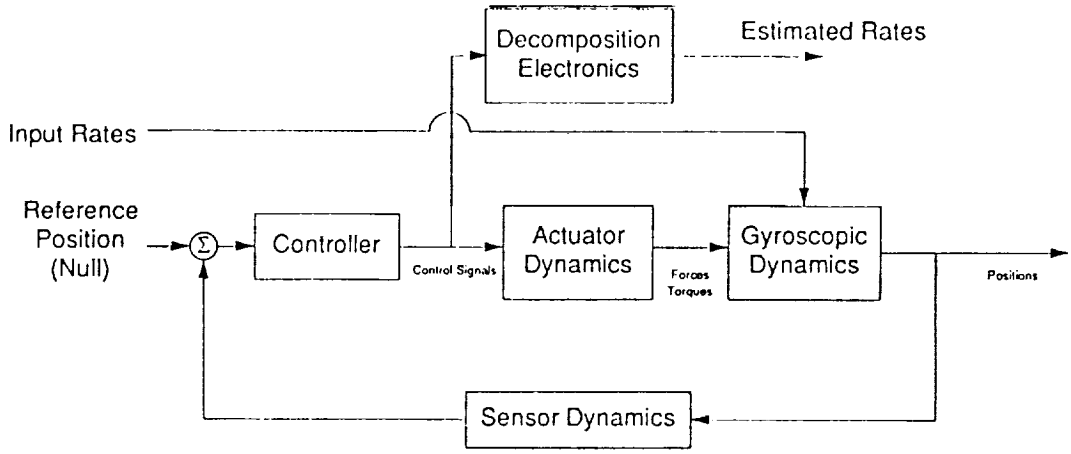

Figure 3. Microgyro Block Diagram.

Angular rotations of the gyro support frame cause torques to be applied to the rotor. The mechanical dynamics of the rotor transform these forces and torques into rotor displacements. Sensors determine these displacements in relation to the reference position and the resulting error signal is sent to a control system. The control system sends the appropriate signals to the actuators, returning the gyro to a null position. Knowledge of the actuator dynamics allows the input rates to be estimated from the actuator control signals.

The device consists of three types of electroquasistatic components - the motor drive, position sensors, and the non-rotary actuators for rebalance and suspension. As with suspended macroscopic gyros, the rotor is spun by a motor to produce angular momentum, suspended and controlled by force and torque actuators, and sensed by various position sensors.

Position control must be effected in both axial and radial directions requiring four sets of actuators, two for the upper and lower axial suspension and two for upper and lower radial rebalance actuator/sensors - and the motor driver actuator. These may be combined so that electrodes are shared. Each active conductive layer of the rotor is composed of structural polysilicon and separated from the other conductive layers by an insulating silicon nitride layer.

Capacitive sensing is used throughout with all sensor electrodes placed below the rotor away from actuating electrodes. The sensors are driven at 100 kHz by SatCon designed electronics.

SPECIFICATIONS AND CONFIGURATION

In order to reduce the complexity of the VLSI and utilize well developing processing techniques, we have reduced the rotor structure geometry to a two layer polysilicon construction sandwiching a thin insulating layer. A total of three polysilicon and three nitride layers are required above the electrodes placed over the substrate. This will reduce the complexity of the control system requirements as well as allow sensing at higher signal to noise ratios.

This design is shown conceptually in Figures 4, 5 and 6. All sensing electrodes will be placed below the rotor over the substrate either as an ion implanted pattern or a "polysilicon #0" layer over nitride. Sensors will detect capacitance between a pair of active electrodes and the disc underside of the rotor. The outer rings (Figure 4) will sense radial deflections in two directions while the inner rings will detect tilting. The upper rotor electrodes will be articulated. Radial forces will provide combined drive torque and radial actuation, while the overhanging axial electrodes will couple with the large area electrodes to provide tilt correction. A variety of geometries will be included on the die.

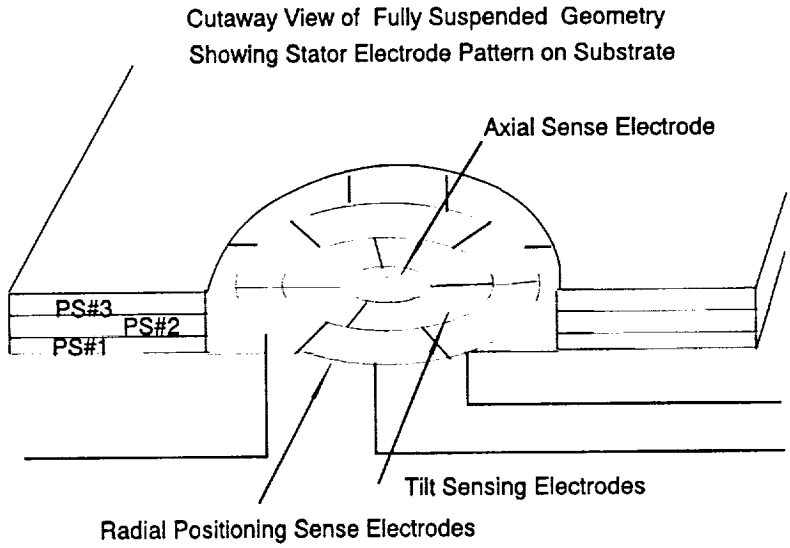

Figure 4. Full Suspended Geometry Showing Sensing Electrodes.

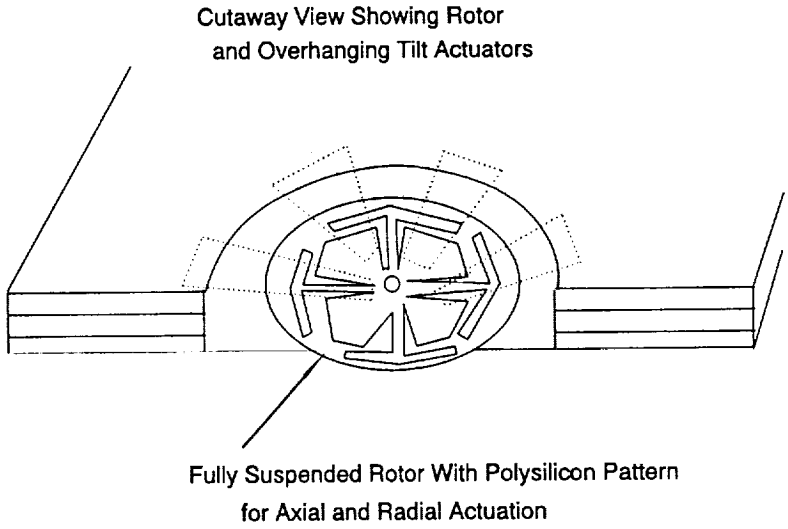

Figure 5. Fully Suspended Geometry Showing Rotor Electrodes.

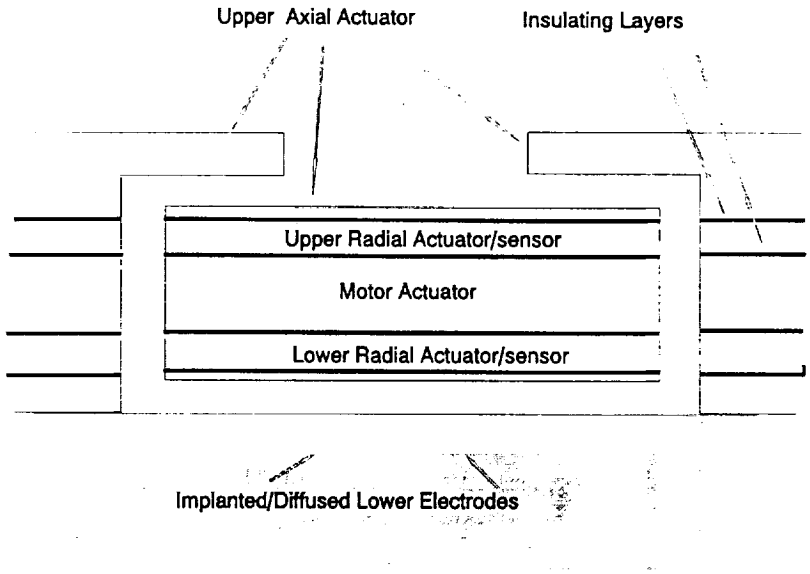

Figure 6. Cross Section Fully Suspended Geometry.

Sizing

The target rotor diameter, 200 μ, was chosen as the largest size that could be fabricated without significant warpage due to residual stress buildup during fabrication. The rotation rate is constrained by stress limits in the rotor and electronics limits in the motor driver circuitry. A rate of 500,000 rpm (8.3 kHz) was chosen as a reasonable extension of current motor rates (about 20,000 rpm). This is well below the ultimate spin rate (about 10,000,000 rpm) determined by material strength limits.

The fabrication of this design requires a total of three layers on the rotor. The top structure which contains the topology for both the upper actuators and the radial and drive actuators should be at least 1-2 μm thick for reasonable actuation forces. The insulating nitride layer can be much thinner than this, say 0.2 μm. The lowest layer (polysilicon) used for sensing interacts axially with substrate pattern and therefore can be as thin as can be stably fabricated.

The axial gap between substrate and rotor is nominally 2 μ. This represents a tradeoff between gap capacitance and rotor unstable frequency but is also influenced by VLSI fabrication considerations. A smaller gap would make sensor measurements more accurate at the cost of raising the unstable frequency and complicating the control problem. The 2 μ gap gives a 300 Hz unstable frequency.

SENSORS

The position sensor mechanism is the electrostatic detection of capacitance. The electrode pattern in the substrate provides enough electrodes to discern radial position and angle, tilt off

rotation axis and overall axial position. Capacitive position sensing is commonly used in macroscopic devices, and has also been successfully applied to other micromechanical devices. The basic concept is to drive a constant current across an air gap (whose capacitance varies inversely with gap distance) and read the resulting voltage which is linearly proportional to the gap. High frequency modulation and demodulation allow good noise immunity. Though the capacitance of the microgyro axial gap will be very small (about 10^{-14} farads), the placement of FETs via a hybrid construction on the silicon substrate as preamplifiers in conjunction with guard wires to the sensing electrodes will allow the dynamic range required to meet the resolution requirements.

ELECTRONICS

Sensor Electronics

The capacitance of the position sensor varies inversely with the distance from the sensor to the target with detectable variations of the order of 10^{-17} F. Any stray capacitance on the sensor leads will affect the linearity of the measurement unless the leads are appropriately guarded. The ability to detect position accurately is also hampered by any load placed on the sensor capacitance by the measurement electronics.

Electrostatic Sensor/Actuator Circuitry

Referring to Figure 7 we see that U12 is VCO/Function Generator IC with triangle, square, and sine wave outputs. R34 and R35 determine the charge-up and charge-down currents into C35. The charge-to and charge-from voltage levels are set by internal references in the ICL8038. This gives a charge/discharge time τ from $E = I\tau/C$ which sets the frequency for a triangle wave. This triangle wave is the input to a diode break point sine wave function generator. Trim Pots R31, R34, and 37 are adjusted to minimize sine wave distortion.

Q1 is a programmable zener diode, which is set up for -5 v. The -5 v. is one end of a 10-turn Pot (R2) and ground is the other. The wiper of the Pot is buffered by U1, and summed with the sine wave from U12 into U2. The Q1, U1, R2 circuit's output is the electrostatic levitation voltage for the rotating disc. Summation output from U2 is the input to U3, which drives one side of a 5 MΩ resistor and one input of a differential amplifier U5.

The other side of the 5 MΩ resistor is connected to the active electrode of the "Cap Gauge" and the input of a low input capacitance unity gain amplifier. Q2, Q3, Q4, Q5, Q6, U4, and U6 are used to implement the low input capacitance unity gain amplifier. Q2A and Q2B are the input differential source followers. Their source impedances are two 200 micro-amp current sources Q4, Q5 and Q6. The source follower's source voltage follows changes in gate voltage (input) by the relationship $g_m R_l/(1+g_m R_l)$. The greater the product $g_m R_l$, the more closely the source follows the gate. R_l in this case is a current source with an output impedance greater than 2 MΩ and the g_m of the FETs is greater than 1000 μmhos, so the source should follow the gate to better than 1 part in a thousand, which means the effective gate-to-source input capacitance is reduced, first order, by a factor of 1000.

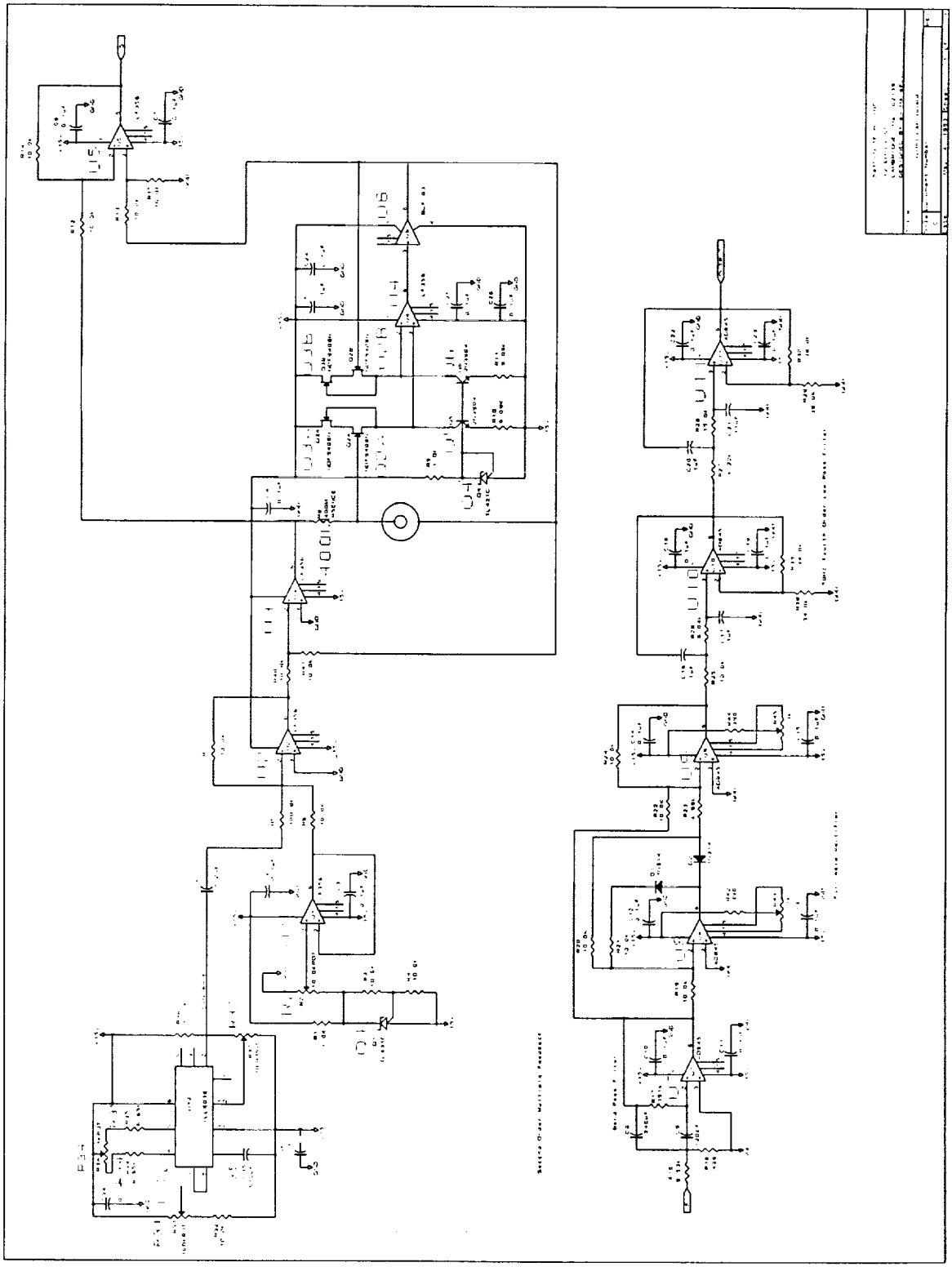

Figure 7. Schematic of Capacitive Sensing/Electrostatic Actuation Electronics.

The sources of Q3 are connected to the drains of Q2, and its gates are connected to the sources of Q2. G_{os} of C2 is less than 2 μmhos, so R_l for source followers Q3 is greater than 500 kΩ which means the drains of C2 will follow the gates of C2 to one part in 500, thus reducing input gate to drain capacitance. With careful layout and guarding a total input capacitance of 50 fF is achievable.

Q2's sources are connected to the inputs of U4, whose output is connected to the input of U6, a high output current buffer. The output of U6 is fed back to the gate of Q2B (amplifier inverting input) to implement unity gain for low capacitance amplifier. U6's output drives the active plate guard, and is fed back to the inverting input of U3, so that the summation output from U3 maintains the summation at the cap gauge active plate. Also, U6's output is connected to the remaining input of differential amp U5. The current that flows through the capacitor which is defined by the active plate area and the distance to the current return plate flows through the 5 MΩ resistor to generate a voltage across the 5 MΩ resistor. This voltage is indirectly measured by differential amp U5. It is proportional to the defined capacitor, and inversely proportional to the distance between the active area plate and the return plate.

The output of U5 is connected to the U7 input of a second-order bandpass filter centered at U12's sine wave frequency. A full wave rectifier (U8, U9, and associated components) rectifies the output of the Band-Pass filter. The rectified signal is then subjected to a 4-pole low-pass filter (U10, U11, and associated components). The output of the 4-pole filter is a DC signal with less than 0.1% carrier ripple.

Motor Drive Electronics

The gyro wheel-motor is a three-phase bipolar variable-capacitance motor. Since this motor type is synchronous, i.e., produces torque only when the rotation frequency and excitation frequency are the same, it requires a variable-frequency drive source. In addition, the push-pull excitation required for each of the three bipolar phases will require six high-voltage output stages. The motor is driven with balanced bipolar voltages so that the rotor will remain near zero potential so that the axial actuators will not require a large DC bias.

Motor start-up will require that the excitation frequency start at the sub-Hertz level and ramp up to the full-speed value of 25 kHz. This is accomplished with a ramp generator and voltage-to-frequency (V/F) converter. The bipolar three-phase generator takes the single-phase output of the V/F converter and produces three square-waves with 120 degrees phase difference and their complementary signal for driving the output stages. In addition, the circuit generates the signal pair which develops the bipolar waveforms. The output circuit contains six high-voltage drivers, one for each bipolar phase, and can deliver up to 120V.

CONTROL DESIGN

One of the goals of the controller is to keep the orientation of the rotor fixed, in the null position, relative to the orientation of the "stator" frame of the gyroscope. In addition, the

controller must provide accurate measurement of the torque that is required to maintain the rotor in the null relative orientation. As usual, the simplest controller that can meet the performance objectives is desired in order to minimize hardware complexity. In particular, a fixed-gain, linear controller is desired that can be easily implemented in analog electronics. This will force some performance and stability robustness tradeoffs, in particular because the plant dynamics are a strong function of the operating speed and are open-loop unstable. Because of the open-loop unstable nature of the plant -- an inverted pendulum at low speeds -- closed-loop control is required from zero speed to the full operational speed. The challenge, then, is to find a fixed gain controller that will provide adequate performance at all speeds.

Modeling

Three sources of torque will be considered in this model, the gravity torque, the motor radial torque, and the actively controlled torque produced by the electrostatic actuators. The motor produces a stabilizing or restoring radial torque. For small angles, this can be linearized to give a stabilizing radial torsional spring. The torsional spring constant for motor under operating voltages is expected to be $\approx -1 \times 10^{-13}$ Nm/rad.

The electrostatic actuators are voltage biased to provide a linear relation between input voltage and torque. The linearized model of these actuators includes, in addition to the voltage induced torque, an "unstable" spring torque that is proportional to the relative orientation of the rotor to the "stator" frame. The unstable torsional spring caused by the actuator (with an associated unstable frequency of 300 Hz) is seen to dominate the stable torsional spring caused by the motor (with an associated stable frequency of 71 Hz).

Open-Loop Dynamics

The variation of the plant dynamics from zero speed to operational speed of 500,000 rpm (8,333 Khz) is dramatic. At zero speed, the plant is a two-degree-of-freedom unstable pendulum. The two by two plant transfer function matrix relating control voltage inputs to rotor orientation output becomes diagonal in this case, with no cross-coupling between the x-direction tilt dynamics and the y-direction tilt dynamics. At zero speed, therefore, the plant can be treated as two identical single-input, single-output (SISO) systems. At frequencies below 300 Hz, the dynamics of this parallel or diagonal transfer function are seen to be dominated by the unstable torsional spring produced by the combination actuator and motor torsional effects. The unstable spring produces the flat low frequency magnitude response between input voltage (torque) and output orientation (angle) with the 180 degrees of phase indicating an unstable spring. At frequencies above the 300 Hz unstable frequency, the transfer function falls off with a slope of minus two, caused by the double integration of torque to angle, and scaled by the voltage to torque constant and the radial moment of inertia of the rotor.

At full speed (500,000 rpm or 8,333 Hz) the plant dynamics are dominated by gyroscopic effects. Because of the x-y symmetry, the two diagonal or parallel transfer functions (x voltage to x orientation and y voltage to y orientation) are the same. Similarly, the two off-diagonal or cross-coupling transfer functions (x voltage to y orientation and y voltage to x orientation) are also the

same. The plant is completely characterized by two transfer functions, the parallel (diagonal) and cross (off-diagonal) transfer functions.

Controller Design

The design approach to develop a fixed-gain controller for this speed varying plant was to first examine how optimal, full-state feedback controllers change with changing plant speed. This full-state feedback controller is then implemented as an output feedback controller using lead-lag compensators to provide estimates of the velocity states.

The first step in this design approach was to develop full-state feedback controllers for various operational speeds. These full-state feedback controllers were designed using the linear-quadratic-regulator (LQR) approach. This controller is the "optimal" initial condition regulator, which closely matches the regulator type performance goals of the controller for the micro-gyroscope.

Both the zero-speed, and full-speed state feedback compensators suffer from performance problems when used over the full speed range. The zero-speed state-feedback compensator exhibits slow decay time and low-bandwidth at full-speed. The full-speed state-feedback compensator becomes unstable at low speeds. By using a combination of these compensators, however, a tradeoff can be effected between high-speed performance and low-speed stability. This procedure involved iteratively trying linear combinations of the zero-speed compensator. The design parameters are the ratio of zero-speed to full-speed feedback gains, and the compensator bandwidths controlled by the cost-on-control-weighing parameters. These parameters were iterated to yield a state-feedback compensator with a minimum of 1000 Hz bandwidth and the largest minimum decay time over the whole speed range. In addition, the ratio between zero-speed and full-speed bandwidth was keep under a factor of 10.

The resulting "best" compensator uses less parallel-proportional gain than the zero-speed design and less cross-proportional gain than the full-speed design. The resulting closed-loop root-locus versus rotational speed is shown in Figure 8 along with the zero-speed case. The "best" compensator has improved damping and decay time compared to the zero-speed case.

Sensor Testbed

A set of structures compatible with the first multi-user run[1] at MCNC was designed around a single nitride, two layer polysilicon process. Masks for key structures and a view of the results are shown in Figures 9 and 10. The rotor geometries will allow testing of the accuracy and response of capacitive sensing circuitry and the effectiveness of guarding and the response to actuation voltages. Additionally, they will serve to acquaint us with the techniques of driving, manipulating, and evaluating micromechanical structures.

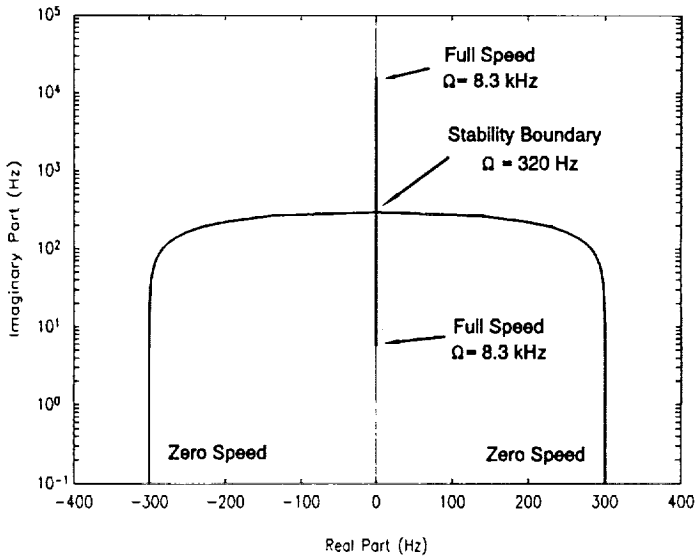

Figure 8. Root-locus of Plant Eigenvalues versus Rotational Speed.

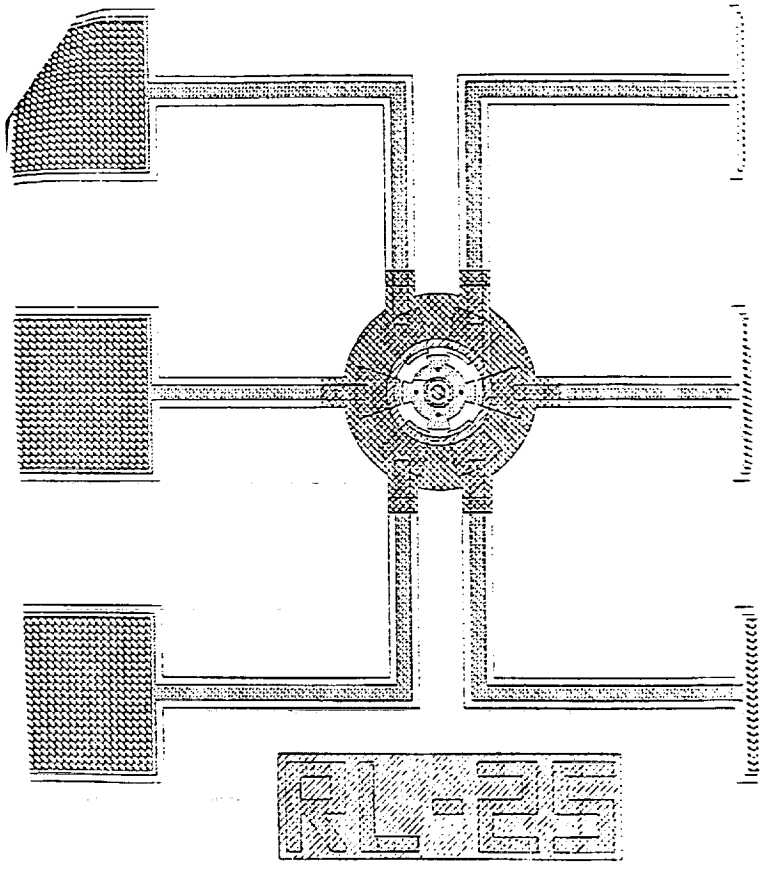

Figure 9. Composite Mask of Bushed Motor.

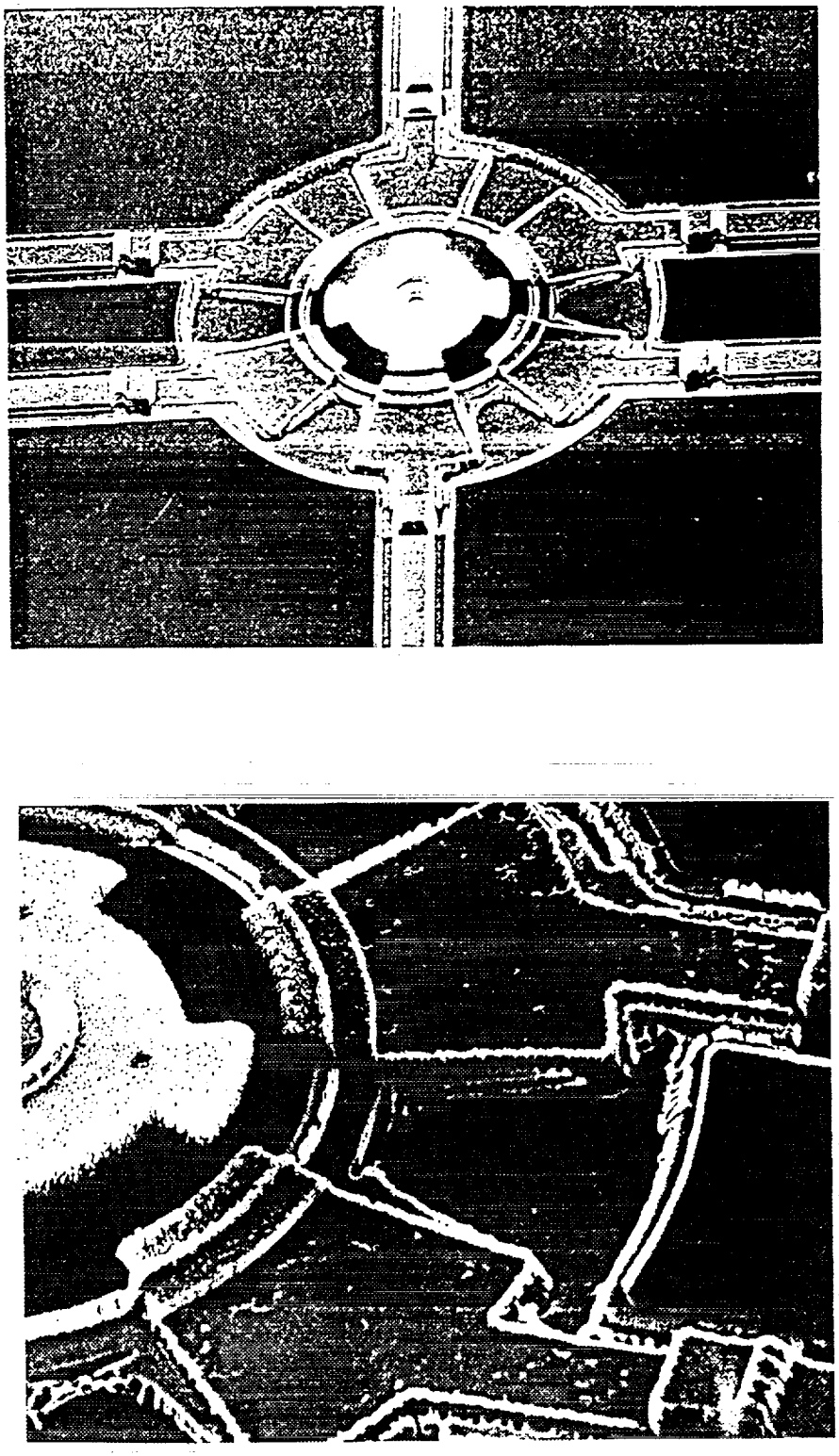

Figure 10. SEM of VLSI Fabricated Motor.

Performance Specifications

A summary of system parameters is given in the table.

Table 1. Microgyro Performance Specifications

Spin Angular Speed	8.3 kHz (500 kRPM)
Spin Moment of Inertia	1.5×10^{-18} kgm-m^2
Precession Moment of Inertia	8×10^{-19} kgm-m^2
Minimum Angular Rate	0.01°/s
Thermal Sensor Noise	$< 0.4 \times 10^{-3}$ v
Angular Sensitivity	< 0.008°
Thermally Limited Rebalance Rate	100 Hz
Sensor Electrode Capacitance	$\sim 3 \times 10^{-14}$ F
Sensor Operating Current (0.5 V)	$\sim 0.4 \times 10^{-9}$ A
Nominal Drive Actuator Potential	5 v
Drive Torque Per Pole	10^{-11} N-m
Viscously Induced Torque	$< 10^{-11}$ N-m
Spindle Friction Torque	0.2×10^{-12} N-m
Rotor Radius	100 μm
Radial Gap	2.0 μm
Vertical Gap	2.0 μm
Rotor Thickness	2.0 μm
# Stator Poles	6
# Rotor Poles	4
Nominal Gap Voltage	0.5 v

1. DARPA sponsored at Microfabrication Center, Research Triangle Park, NC. Dies were delivered in April.